Nitrate Anions and Ion Pairing at the Air−Aqueous Interface†

Man Xu, Cheng Y. Tang, Aaron M. Jubb, Xiangke Chen, and Heather C. Allen*

Department of Chemistry, The Ohio State University, 100 W. 18th Avenue, Columbus, Ohio 43210

Received: June 18, 2008; Revised Manuscript Received: October 31, 2008

Nitrate ions are ubiquitous in aqueous-phase atmospheric aerosols from the polluted to the remote troposphere and are involved in a variety of atmospheric reactions. Thus, a fundamental understanding of nitrate ions at the air−aqueous interface is of prime importance with respect to understanding atmospheric aerosol chemistry. In the present study, investigations of the air−aqueous interface of a series of divalent metal-nitrate solutions, $Mg(NO_3)_2$, $Ca(NO_3)_2$, and $Sr(NO_3)_2$, were carried out using vibrational sum frequency generation (VSFG) spectroscopy. The vibrational symmetric stretch mode of nitrate ions at the air−aqueous interface (1047 cm^{-1} and 1063 cm^{-1}) was directly probed. Analysis of the VSFG spectra reveals the perturbation from cation−anion interactions on interfacial nitrate ions. Ion pairing between interfacial nitrate anions and divalent metal cations follows the same trend as bulk ion pairing: $Sr^{2+} > Ca^{2+} > Mg^{2+}$. Moreover, nitrate anions in the air−aqueous interfacial region are found to be relatively free from Coulombic effects of Mg^{2+} cations for $Mg(NO_3)_2$ concentrations with at least seven hydrating water molecules on average per ion.

Introduction

Recently, the nature of nitrate ions at the aqueous interface has received attention because of the growing awareness of their key role in the surface chemistry of atmospheric aerosols.[1−4] Nitrate is pervasive in the atmosphere in the form of nitrate radicals and nitrate ions. Nitrate radicals have been studied extensively with respect to their role in night-time gas-phase atmospheric chemistry.[5,6] Like the gas-phase nitrate radical in the atmosphere, the aqueous-phase nitrate ion is a common constituent of atmospheric aerosols. Gaseous ammonia reacts with nitric acid in the atmosphere and forms aerosol-phase ammonium nitrate. The generated nitrate aerosols are in the aqueous state at relative humidity conditions above the deliquescence.[7] In marine regions, the formation of the nitrate ion is associated with significant chloride ion depletion in sea salt aerosols as a result of NaCl reaction with HNO_3, NO_3 radicals, N_2O_5, and $ClONO_2$.[5,8,9] Water-induced recrystallization of nitrate on NaCl surfaces into $NaNO_3$ crystallites avoids passivation of the surface and further depletes chloride ions.[1,9] The gaseous halogen products generated are photochemically active and are involved in ozone destruction and/or formation and in reactions with organics in the troposphere.[8,9] Such chemistry is of significant importance in marine urban regions.[1,9] In polar regions, recent studies have indicated that elevated nitrogen oxides and hydroxyl radical levels in and above snowpacks originate from the photolysis of nitrate ions in snow and ice (possibly involving the quasi-liquid layer on the ice surface) and may ultimately affect global chemical composition.[2,8,10] Thus a fundamental understanding of the air−aqueous nitrate interface may provide insight into the role of nitrate ions at the surface of aqueous-phase atmospheric aerosols and atmospheric heterogeneous reaction mechanisms.

Computational studies have predicted interesting results concerning the propensity of nitrate ions for the air−aqueous interface.[3,4,11,12] Salvador et al. proposed that the nitrate ion might prefer interfacial over bulk solvation,[11] whereas Dang et al. predicted that the nitrate ion was preferentially localized below the Gibbs dividing surface.[3] The Gibbs dividing surface is where the interfacial water density is half its bulk value. More recent molecular dynamics (MD) simulations suggested that nitrate exhibits a very weak surface propensity and a small amount of nitrate ions reside at the air−aqueous interface.[4,12] In these MD simulations, the terms interface and surface are used interchangeably, both referring to the region around the Gibbs dividing surface.[3,4,11,12]

In the work reported here, for the first time, a vibrational mode of the nitrate ion at the air−aqueous interface is directly probed by an interface-specific technique, vibrational sum frequency generation (VSFG) spectroscopy. (The term interface in VSFG studies refers to where there is lack of inversion symmetry.[13]) Kido Soule et al.[14] have studied nitric acid in a different spectral region. Other previous VSFG studies of nitrate aqueous solutions mainly focused on the influence of ions on the interfacial water structure.[15] Our VSFG study directly probes nitrate at the interface and reveals that the interfacial nitrate anion follows bulk ion pairing trends with Mg^{2+}-nitrate ion pairing weaker than Ca^{2+}−nitrate and Sr^{2+}−nitrate ion pairing.[16] Ion pairing refers to the interaction and association of oppositely charged ions,[17,18] where the long-range electrostatic Coulombic forces play a major role.[17]

However, $Mg(NO_3)_2$ is particularly interesting at the air−aqueous interface. We observe here two distinct nitrate populations for aqueous $Mg(NO_3)_2$ solution interfaces, where the population provides information on the extent of ion−ion interaction. The amount of relatively free nitrate ions (negligible ion−ion interaction) at the air−aqueous interface becomes significant for $Mg(NO_3)_2$ concentrations with at least seven water molecules hydrating each ion on average. This phenomenon is not observed in the bulk. At the air−aqueous interface, it appears that the number of water molecules available to solvate the nitrate ion plays a pivotal role for ion pairing, or lack of it.

† Part of the special section "Physical Chemistry of Environmental Interfaces".

* To whom correspondence should be addressed. allen@chemistry.ohio-state.edu.

10.1021/jp805376x CCC: $40.75
Published on Web 12/10/2008

Experimental Section

VSFG Instrumentation. The VSFG spectra were acquired using a 20 Hz scanning VSFG system (EKSPLA). The VSFG experiments were carried out using a visible beam at 532 nm and an infrared beam tunable from 1000 to 4000 cm^{-1}. The 532 nm visible beam is generated by doubling the frequency (second harmonic) of the 1064 nm pump source from an Nd:YAG laser (27 ps pulse duration and 20 Hz repetition rate, EKSPLA, PL 2143A/20/SS). The tunable infrared beam is generated from an optical parametric generator (EKSPLA, PG401/DFG2-16P) using a $AgGaS_2$ crystal to generate the difference frequency for the infrared generation. The 532 nm light is focused 40 mm after the sample surface by using a plano convex lens (700 mm focal length). At the sample surface the 532 nm light has a diameter of 1 mm and an intensity of ~400 μJ/pulse. The infrared beam is focused at the sample surface by using a ZnSe lens (50 mm focal length) to yield a <0.5 mm beam diameter of the infrared light at the sample surface with an intensity of ~40 μJ/pulse at 1050 cm^{-1}. The input angles for the 532 nm and infrared beams are 60° and 55° from the surface normal, respectively. The 532 nm and infrared beams are overlapped at the interface spatially and temporally. The resulting sum frequency light is collected using a cooled charge-coupled device (CCD) camera (Andor Technology, DV412) after passing through a monochromator. The polarizations were ssp for the sum frequency, visible and infrared beams, respectively. The s polarized light has its electric field vector perpendicular to the plane of incidence, while the p polarized light has its electric field vector parallel to the plane of incidence. In addition ppp polarization VSFG spectra were acquired. These spectra did not show any differences in the frequencies observed from the ssp polarization spectra. The VSFG spectra were acquired using a 30 s exposure time for each data point and are an average of four to six replicate spectra. (VSFG spectra of lower concentration solutions are shown in the Supporting Information.) The IR profile was used to normalize the VSFG spectra since the IR was detected in real-time with the VSFG intensity. To ensure the stability of the VSFG system and to confirm the reproducibility of the spectra, VSFG spectra of an 8.0 mM sodium dodecyl sulfate (SDS) solution were obtained at the beginning and at the end of each experiment. (Note that the overall lower VSFG intensity of the 3.3 m spectrum should not be compared to the 2.6 m overall spectral intensity since we have determined that the sample height was not adequately reproduced between these spectral acquisitions. As shown in our Supporting Information, the overall intensity of the main 1047 cm^{-1} peak decreases with decreasing nitrate concentration as one would expect from bulk studies.)

Raman Instrumentation. Raman spectra presented in this paper were obtained by passing the unpolarized 785 nm light from a continuous wave laser (Raman System Inc.) onto the sample using a 7.5 mm focusing Raman probe (InPhotonics, RPS785/12-5). The Raman scatter was focused onto the entrance slit of a 500 mm monochromator (Acton Research, SpectraPro SP-500) through a fiber optic imaging coupler (Acton Research, FC-446-030), dispersed by a 600 groove/mm grating blazed at 1 μm, and collected on a liquid nitrogen cooled CCD camera (Roper Scientific, LN400EB, 1340 × 400 pixel array, back-illuminated and deep depletion). The power of the 785 nm beam was ~240 mW. The slit width of the monochromator entrance slit was set to 50 μm, and the resolution was 3.2 cm^{-1}. Raman spectra were collected with an exposure time of 50 s. Before data collection, the monochromator was calibrated using the 435.833 nm Hg line of a fluorescent light and was verified by comparison to the Raman spectrum of naphthalene.

Infrared Instrumentation. Attenuated total reflection Fourier transform infrared (ATR-FTIR) spectra were obtained using a Thermo Nicolet FTIR spectrometer (Thermo Electron Corporation, Avatar 370). ATR-FTIR instead of transmission FTIR was used as a bulk probe in the present study for ease of acquiring spectra. IR perturbation depth for ATR-FTIR is on the order of the wavelength of light, and the IR absorption is therefore dominated by the bulk. We have assumed that the refractive indices of aqueous solutions are relatively constant. A 45° single-bounce ZnSe crystal trough mounted on an accessory (Thermo Electron Corporation, Smart SpeculATR) was employed to collect spectra at a spectral resolution of 4 cm^{-1}. The spectra shown in the present paper were averaged over 128 scans.

Chemicals. All nitrate salts were purchased from Fisher Scientific. The aqueous solutions were made using Nanopure water with resistivity 18.0−18.3 MΩ cm, and filtered, typically 3−6 times, using a carbon filter (Whatman Carbon-Cap 150) to remove organic impurities. Raman analysis using a calibration curve of unfiltered concentrations for determining concentrations after filtration was completed (filtration also removes some of the ions in addition to organic molecules). VSFG spectra in the 2800−3000 cm^{-1} region were obtained to check for organic impurities in the salt solutions.

Molality (m), which is defined as the moles of solute per kg of water, is used as the concentration unit for the nitrate salt solutions. Aqueous solutions of 2.6 and 3.3 m were studied in the present work. (Lower concentrations were also studied and their spectra are shown in the Supporting Information.) 2.6 m corresponds to 0.045 × (salt mole fraction) and 3.3 m corresponds to 0.056 × for all salts.

Results and Discussion

Relatively high concentrations, 3.3 and 2.6 m, of nitrate salts were studied here. Lower concentration spectra (shown in the Supporting Information) also reveal a higher frequency resonance as that found for the 2.6 m nitrate salts. Anomalous air−aqueous interfacial behavior is observed spectroscopically when comparing the 3.3 m $Mg(NO_3)_2$ solutions, 6 solvating water molecules per ion, to the 2.6 m $Mg(NO_3)_2$ solutions, 7 solvating water molecules per ion. This anomalous behavior is not observed in the bulk as studied by Raman and infrared spectroscopies.[16]

Figure 1 shows the ssp-polarized VSFG spectra of $Mg(NO_3)_2$ aqueous solutions at the air−aqueous interface. In the spectrum of the 2.6 m (0.045 ×) $Mg(NO_3)_2$ aqueous solution (Figure 1a), a peak at 1063 cm^{-1} and a shoulder at 1047 cm^{-1} are observed, whereas in the spectrum of the 3.3 m (0.056 ×) $Mg(NO_3)_2$ solution (Figure 1b) the dominant peak position is at 1047 cm^{-1}. To assign the observed VSFG peaks, Raman and IR spectra were obtained from the $Mg(NO_3)_2$ aqueous solutions, as shown in Figure 2. The peaks at 1050 cm^{-1} in the Raman spectra (Figure 2a) and 1044 cm^{-1} in the IR spectra (Figure 2b) are assigned to the symmetric stretch mode of nitrate. For free nitrate with a D_{3h} symmetry, the symmetric stretch band is IR inactive.[19,20] The symmetric stretch however occurs in the IR spectra (Figure 2b) as a result of the perturbation of cations and/or water molecules that lowers the symmetry of nitrate.[19−21] The noncoincidence between Raman and IR frequencies may arise from the strong intermolecular resonant vibrational coupling that leads to rapid transfer of vibrational excitations in the time domain and delocalization of vibrational modes in

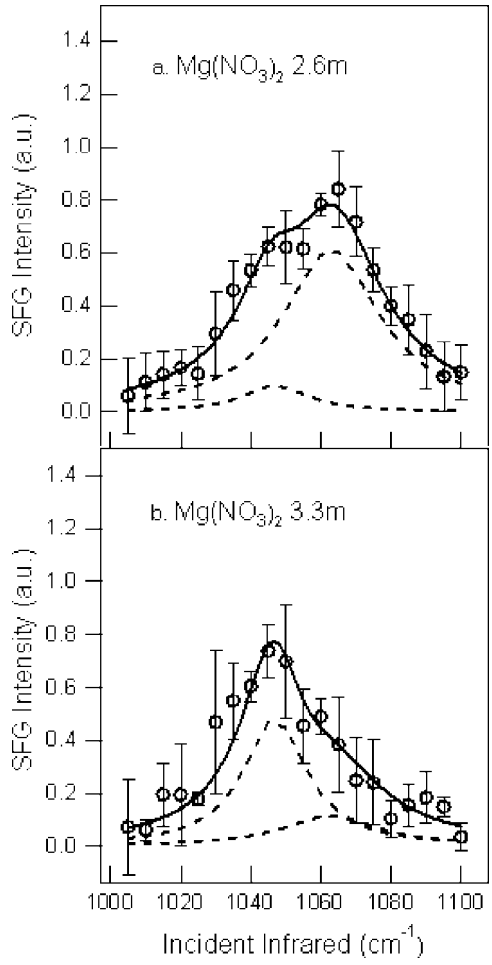

Figure 1. VSFG spectra of aqueous $Mg(NO_3)_2$ solutions with ssp polarization: (a) 2.6 *m* $Mg(NO_3)_2$; (b) 3.3 *m* $Mg(NO_3)_2$. Circles: experimental data with error bars; solid lines: overall fits; dashed lines: Lorentzian component peaks.

the frequency domain.[22,23] Therefore, the peaks around 1047 cm^{-1} and 1063 cm^{-1} in the VSFG spectra of $Mg(NO_3)_2$ (Figure 1) are assigned to the symmetric stretch mode of nitrate anions at the air−aqueous interface.

In Figure 1a and b, the dominant VSFG peak position of the nitrate symmetric stretch has changed from 1063 to 1047 cm^{-1} as the bulk concentration of $Mg(NO_3)_2$ increases from 2.6 to 3.3 *m*. Unlike VSFG spectra that provide vibrational information at the interface, Raman and IR spectra shown in Figure 2 provide bulk information. Raman spectra (Figure 2a) show only a slight frequency shift of the nitrate symmetric stretch band from 1049 to 1050 cm^{-1} when $Mg(NO_3)_2$ concentration increases from 2.6 to 3.3 *m*. Lower concentration Raman spectra do not reveal any additional shift.[16] In the IR spectra (Figure 2b), a similar frequency shift (from 1044 to 1045 cm^{-1}) is observed. When the concentration of $Mg(NO_3)_2$ varies in a much broader range (0.5 *m* to saturated), the frequency shift is less than 2 cm^{-1} (spectra not shown here). Note that in both Raman and IR spectra the symmetric stretch peak shifts 1−2 cm^{-1} to higher frequency with increasing concentration. This blue shift has been interpreted as the weakening of nitrate−water hydrogen-bonding.[16,24] In the VSFG spectra, there are two resolvable component peaks that are 16 cm^{-1} apart, where the 1063 cm^{-1} peak and the 1047 cm^{-1} peak are dominant for the 2.6 and 3.3 *m* $Mg(NO_3)_2$ solutions, respectively. The VSFG shift in frequency for the dominant peak is opposite to what is observed in the bulk studies. Therefore, the 16 cm^{-1} frequency change of the nitrate symmetric stretch band in the VSFG spectra cannot be simply explained by a bulk-like ion pairing trend. Only the 3.3 *m* symmetric stretch frequency is similar to the observed bulk symmetric stretch frequencies, whereas the 2.6 *m* symmetric stretch frequency has never before been observed for either interfacial or bulk aqueous $Mg(NO_3)_2$. However, this frequency has been observed while studying droplets under low relative humidity conditions. The low relative humidity conditions caused dehydration not possible in a bulk solution.[25] Clearly, at the lower 2.6 *m* solution air−aqueous interface, unique behavior is observed. Deconvolution of the symmetric stretch peak further confirms a two-component band, which we assign to two different populations.

At the air−aqueous interface, the two populations associated with the component bands at 1047 and 1063 cm^{-1} are assigned to ion-paired and relatively free nitrate, respectively. Nitrate anions located in the air−aqueous interfacial region attract Mg^{2+} cations toward the interface. This interface-driving electroneutrality force competes with the bulk-driving electrostatic force.[12,26]

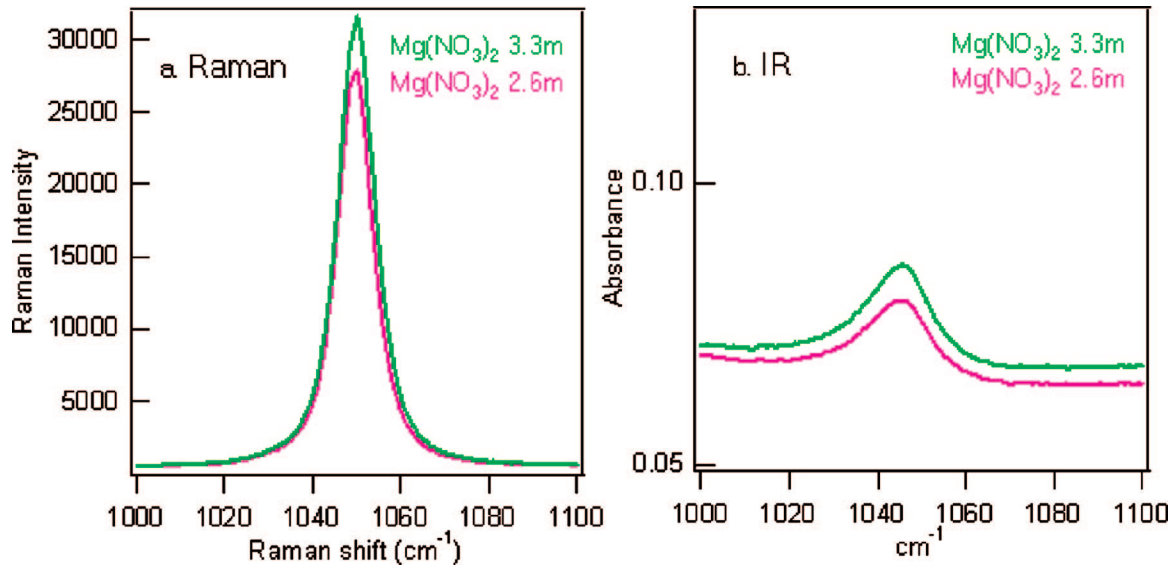

Figure 2. Raman and IR spectra of aqueous $Mg(NO_3)_2$ solutions with concentration 2.6 and 3.3 *m*: (a) Raman spectra; (b) IR spectra. Coloring scheme: 2.6 *m* $Mg(NO_3)_2$, pink; 3.3 *m* $Mg(NO_3)_2$, green.

TABLE 1: Curve-Fitting Results of Nitrate VSFG Spectra[a]

		nonresonant terms							
	molality (m)	real	imaginary	I_{1047}	hwhm_{1047}	I_{1063}	hwhm_{1063}	I_{1047}/I_{1063}	$\text{SDR}_{\text{IP/free}}$
$Mg(NO_3)_2$	2.6	0.002	0.01	2.9	10.9	25.0	16.8	0.12	0.34
	3.3	0.002	0.01	14.1	10.9	4.7	16.8	3.0	1.7
$Ca(NO_3)_2$	2.6	0.002	0.01	13.0	10.9	2.2	16.8	5.9	2.4
	3.3	0.002	0.01	16.8	10.9	2.1	16.8	8.0	2.8
$Sr(NO_3)_2$	2.6	0.002	0.01	12.5	10.9	1.3	16.8	9.6	3.1
	3.3	0.002	0.01	18.3	10.9	0.91	16.8	20	4.5

[a] Surface number density ratio of ion-paired to relatively free nitrate ($\text{SDR}_{\text{IP/free}}$) is shown. hwhm: half width at half maximum.

According to previous theoretical and experimental studies, $Mg(NO_3)_2$ aqueous solutions are well-behaved, close-to-ideal solutions with extensive ion−water mixing and virtually no formation of contact ion pairs between Mg^{2+} and nitrate.[12,16,21] At the air−aqueous interface, nitrate anions exhibit only a very weak propensity for the interface, as suggested by previous MD simulations.[4,12,26] The VSFG data presented here reveal that the electroneutrality effect of nitrate on Mg^{2+}, within the interface, is relatively weak, and the electrostatic repulsion of Mg^{2+} from the interface dominates. It is well accepted that small "hard" Mg^{2+} ions are strongly repelled from the air−aqueous interface, in accordance with classical theory of electrolyte surfaces.[12,27] In the 2.6 m $Mg(NO_3)_2$ aqueous solution, Mg^{2+} cations reside preferentially deep in the bulk. The Coulombic interaction and the ion pairing between Mg^{2+} and interfacial nitrate are relatively weak, as just discussed. A lack (or significant weakening) of interaction would reasonably shift the nitrate symmetric stretch to higher frequency compared with the nitrate ions where the interaction is stronger at the air−aqueous interface (in the 3.3 m $Mg(NO_3)_2$ solution). Recently, Thomas et al.[4] found that for nitrate anions that approach the air−aqueous interface, there is a decrease in the number of water molecules coordinating to the interfacial nitrate relative to the bulk nitrate. The low coordination number could shift the nitrate symmetric stretch peak to higher frequency compared to the bulk. However, this would also be expected to occur for the 3.3 m $Mg(NO_3)_2$ solution but is not observed in the VSFG spectrum (Figure 1b). In fact, the 1047 cm^{-1} peak position that dominates the 3.3 m solution is close to what is observed in bulk studies. Therefore, we conclude that the electrostatic repulsion of Mg^{2+} from the interface is an important, and possibly dominant effect that results in a weak Columbic interaction between Mg^{2+} and interfacial nitrate for the 2.6 m $Mg(NO_3)_2$ solution. However, it is also likely that surface nitrate dehydration, although not an intuitive result, may be occurring for a more surface active nitrate ion. Nitrate dehydration was observed as the result of low relative humidity in the atmosphere around a droplet (thereby increasing the bulk concentration) using a bulk probe, Raman spectroscopy.[25] Hence, at the air−aqueous interface, the VSFG frequency at 1063 cm^{-1} is assigned to the symmetric stretch of relatively free and dehydrated interfacial nitrate species, and the component peak at 1047 cm^{-1} is assigned to the symmetric stretch of ion-paired interfacial nitrate, likely a solvent-separated ion pair (SSEIP) or a solvent-shared ion pair (SSHIP).

The 1063 cm^{-1} peak has not been observed from bulk Raman or infrared $Mg(NO_3)_2$ ion pairing studies, although it has been observed for the low relative humidity droplet Raman studies mentioned above.[25] The assignment of this peak frequency to a relatively free and dehydrated nitrate anion allows us to further shed light on bulk studies. Although Mg^{2+} has been considered to be ineffective at ion pairing with nitrate from previous bulk studies,[21,28] it is not. This is demonstrated by the present work, which reveals that ion pairing (SSEIP or SSHIP, not a contact IP) dominates at the air−aqueous interface of the 3.3 m $Mg(NO_3)_2$ solution, and provides additional reference frequencies for perturbed nitrate. Therefore, we also conclude that ion−ion interactions are stronger than previously thought in bulk $Mg(NO_3)_2$ aqueous solutions. Zhang et al.[25] postulated an increase in contact ion pairing from their droplet work; however, it is more likely that the dehydration of the nitrate is the driving factor in their observed frequency shift from the bulk Raman spectroscopy. In their droplet study, ions must be approaching each other since water is forcibly being removed in addition to the ion dehydration. Yet when compared to our observations in the VSFG work, it is clear that dehydration is more likely the dominant factor for the observed frequency blue shift.

To better understand the VSFG spectra of 2.6 and 3.3 m $Mg(NO_3)_2$ solutions, curve-fitting analysis was completed for the nitrate symmetric stretch mode. Component peaks at 1047 and 1063 cm^{-1} were employed in the curve-fitting analysis using eqs 1−3 below.

$$I_{\text{VSFG}} \propto |\chi^{(2)}_{\text{eff}}|^2 I(\omega_{\text{vis}}) I(\omega_{\text{IR}}) \tag{1}$$

$$\chi^{(2)} = \chi^{(2)}_{\text{NR}} + \sum_{\nu} \chi^{(2)}_{\nu} \tag{2}$$

$$\chi^{(2)}_{\nu} \propto \frac{A_{\nu}}{\omega_{\text{IR}} - \omega_{\nu} - i\Gamma_{\nu}} \tag{3}$$

The VSFG intensity, I_{VSFG}, is proportional to the absolute square of the effective sum frequency susceptibility $\chi^{(2)}_{\text{eff}}$, which is proportional to the surface number density. I_{VSFG} is also proportional to the intensities of the visible and infrared incident pulses, $I(\omega_{\text{vis}})$ and $I(\omega_{\text{IR}})$. $\chi^{(2)}_{\text{eff}}$ includes the Fresnel factors. In comparing the VSFG spectra in this work, all Fresnel factors were constant (all spectra were obtained using the same beam geometry), therefore, $\chi^{(2)}$ is used for $\chi^{(2)}_{\text{eff}}$. The macroscopic second-order nonlinear susceptibility, $\chi^{(2)}$, is comprised of a nonresonant term, $\chi^{(2)}_{\text{NR}}$, and the sum of resonant terms, $\chi^{(2)}_{\nu}$. A single resonant susceptibility term $\chi^{\nu}_{(2)}$ is described by eq 3 in which A_{ν} is the amplitude of the VSFG transition moment of the vibrational mode ν, ω_{ν} is the center frequency of the transition, and Γ_{ν} is the half-width at half-maximum (hwhm) of the transition. In order to properly compare the fitting results, the real and imaginary nonresonant terms encompassed in $\chi^{(2)}_{\text{NR}}$ and the component peak widths, Γ_{ν}, were held constant.

Curve-fitting results are presented in Table 1, and component peaks are shown as dashed lines in Figure 1. In the VSFG spectrum of 2.6 m $Mg(NO_3)_2$, the component peak at 1063 cm^{-1} is the dominant peak, and the area ratio of the peak at 1047 cm^{-1} to the peak at 1063 cm^{-1} is 0.12. VSFG intensity is related to orientation and is proportional to the square of the interfacial number density (in eq 1). Assuming that the interfacial nitrate orientation relative to the surface normal remains constant for relatively free and ion-paired nitrate,[4] the surface number density

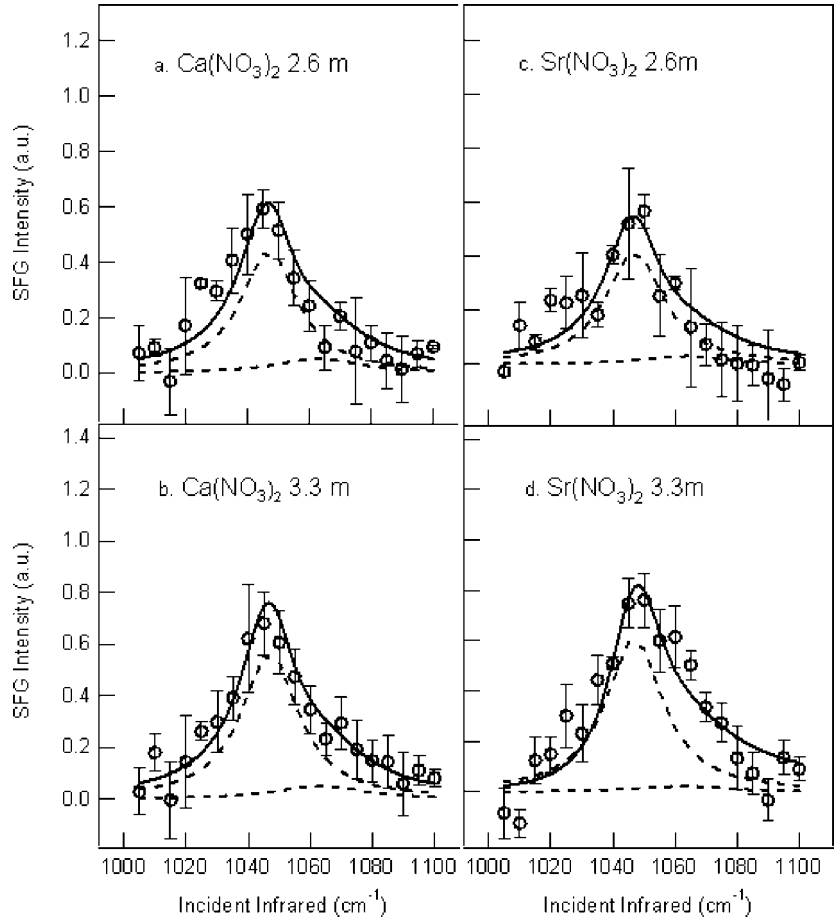

Figure 3. VSFG spectra of aqueous $Ca(NO_3)_2$ and $Sr(NO_3)_2$ solutions with ssp polarization: (a) 2.6 *m* $Ca(NO_3)_2$; (b) 3.3 *m* $Ca(NO_3)_2$; (c) 2.6 *m* $Sr(NO_3)_2$; (d) 3.3 *m* $Sr(NO_3)_2$. Circles: experimental data with error bars; solid lines: overall fits; dashed lines: Lorentzian component peaks.

ratio of ion-paired to relatively free nitrate ($SDR_{IP/free}$) is therefore 0.34. In other words, the majority of interfacial nitrate ions are relatively free at the air−aqueous interface of a 2.6 *m* $Mg(NO_3)_2$ aqueous solution. Lower concentration solutions were also investigated (Supporting Information), revealing that this phenomenon is also observed when increasing the number of solvating water molecules.

As the concentration of the $Mg(NO_3)_2$ solution increases, the Coulombic interaction as well as the ion pairing, SSEIP or SSHIP, between Mg^{2+} cations and interfacial nitrate anions becomes stronger and the number of water molecules available for ion solvation decreases. Note that the 2.6 *m* (0.045 ×) solution has approximately one more water molecule per ion relative to the 3.3 *m* (0.056 ×) solution, that is, at 2.6 *m* there are seven water molecules per ion (cation or anion), and at 3.3 *m* there are six water molecules per ion. At concentration 3.3 *m*, more Mg^{2+} cations are forced to approach the air−aqueous interface relative to the 2.6 *m* solution. The interfacial nitrate is therefore more ion-paired for the 3.3 *m* $Mg(NO_3)_2$ solution. According to our curve-fitting results (Table 1, Figure 1b), the $SDR_{IP/free}$ is 1.7 at the air−aqueous interface of 3.3 *m* $Mg(NO_3)_2$. Thus, the ion-paired nitrate, SSEIP or SSHIP, becomes the dominant interfacial species at the air−aqueous interface of the 3.3 *m* $Mg(NO_3)_2$ solution.

The VSFG spectra of $Ca(NO_3)_2$ and $Sr(NO_3)_2$ solutions at the air−aqueous interface are somewhat different relative to the $Mg(NO_3)_2$ solutions. The VSFG spectra of $Ca(NO_3)_2$ and $Sr(NO_3)_2$ with concentrations 2.6 and 3.3 *m* are shown in Figure 3. According to these spectra, the dominant symmetric stretch peak of nitrate is at 1047 cm^{-1} rather than 1063 cm^{-1}. Hence, the dominant interfacial nitrate species are ion-paired rather than free for $Ca(NO_3)_2$ and $Sr(NO_3)_2$ solutions. Clearly, it is difficult to confirm the existence of a 1063 cm^{-1} peak in these spectra; however, curve fitting with two component bands, 1047 and 1063 cm^{-1}, does reproducibly provide a value for the higher frequency peak in each spectrum of Figure 3. This then gives us an estimate of relative populations of the ion-paired to relatively free nitrate species ($SDR_{IP/free}$) for the $Ca(NO_3)_2$ and $Sr(NO_3)_2$ aqueous surfaces.

As shown in Table 1 along with the fit parameters, if we compare $Mg(NO_3)_2$, $Ca(NO_3)_2$, and $Sr(NO_3)_2$ with the same concentration, 3.3 *m*, the VSFG results show that the $SDR_{IP/free}$ is 1.7 for $Mg(NO_3)_2$, 2.8 for $Ca(NO_3)_2$, and 4.5 for $Sr(NO_3)_2$. At the air−aqueous interface, the strong Coulombic cation−nitrate interaction results in more ion-paired nitrate for $Sr(NO_3)_2$ and $Ca(NO_3)_2$ solutions compared to $Mg(NO_3)_2$ solution of the same concentration. The trend of the Coulombic interaction with nitrate, $Sr^{2+} > Ca^{2+} > Mg^{2+}$, is similar to previous bulk ion pairing studies,[16,20,28] where Ca^{2+} and Sr^{2+} have been found to have a stronger tendency to form ion pairs with NO_3^- in aqueous solutions, with Sr^{2+}−nitrate ion pairing slightly stronger than Ca^{2+}−nitrate ion pairing.

Conclusions

The air−aqueous interface of divalent metal−nitrate solutions was investigated using vibrational sum frequency generation spectroscopy. The symmetric stretch mode of interfacial nitrate at 1047 cm^{-1} was probed for the first time. Moreover, a band at 1063 cm^{-1} was detected from the 2.6 *m* (0.045 ×) $Mg(NO_3)_2$

aqueous solution surface. This resonance has never before been observed in interfacial studies nor in bulk studies of aqueous $Mg(NO_3)_2$, although it has been observed for low relative humidity droplet studies that forcibly dehydrated the ions.[25] Our VSFG studies reveal a lack of ion−ion interaction, and thus, lack of ion-pairing at the air−aqueous interface for a 2.6 *m* (0.045 ×) aqueous solution of $Mg(NO_3)_2$ and for lower concentrations as well. The results also suggest that full solvation, or lack of it, at the air−aqueous interface of $Mg(NO_3)_2$ solutions has significant implications for ion pairing between interfacial nitrate and the small, densely charged Mg^{2+} cation, but not in the manner that is expected. As more water is available, weak Coulombic forces allow cation−anion separation and then allow the more surface active nitrate to become dehydrated (due to the surface activity). The interface appears to be highly sensitive, particularly when enough water is present for Coulombic forces to be adequately shielded. When there is a reduction in ion hydration (no more than 6 water molecules per ion) from concentrating the solution, magnesium and nitrate ions approach one another near the water surface, in the interfacial region. Adding an additional water molecule allows Mg^{2+} to further bury itself toward the bulk, allowing nitrate to exist with minimal perturbation from Mg^{2+}. Dehydration of nitrate occurs as the anion approaches the surface, which is then observed by a significant blue shift in the nitrate symmetric stretch. The fact that relatively free nitrate anions exist at the air−aqueous interface is surprising.

Acknowledgment. We gratefully acknowledge funding of this work from the Department of Energy (DOE-BES, DE-FG02-04ER15495).

Supporting Information Available: The concentrations of nitrate salt solutions in units of m, ×, and M, the Raman and IR symmetric stretch intensities versus nitrate concentration (M), and additional VSFG spectra at several other concentrations and the acquisition parameters. This material is available free of charge via the Internet at http://pubs.acs.org.

References and Notes

(1) Hoffmann, M. R.; Laskin, A.; Finlayson-Pitts, B. *J. Aerosol Sci.* **2004**, *35*, 869–887.
(2) Boxe, C. S.; Colussi, A. J.; Hoffmann, M. R.; Perez, I. M.; Murphy, J. G.; Cohen, R. C. *J. Phys. Chem. A* **2006**, *110*, 3578–3583.
(3) Dang, L. X.; Chang, T.-M.; Roeselova, M.; Garrett, B. C.; Tobias, D. J. *J. Chem. Phys.* **2006**, *124*, 066101.
(4) Thomas, J. L.; Roeselova, M.; Dang, L. X.; Tobias, D. J. *J. Phys. Chem. A* **2007**, *111*, 3091–3098.
(5) Finlayson-Pitts, B. J., Jr. *Science* **1997**, *276*, 1045–1052.
(6) Finlayson-Pitts, B. J.; PittsJr., J. N. *Chemistry of the Upper and Lower Atmosphere: Theory, Experiments and Applications*; Academic Press: San Diego, CA, 2000.
(7) Bauer, S. E.; Koch, D.; Unger, N.; Metzger, S. M.; Shindell, D. T.; Streets, D. G. *Atmos. Chem. Phys.* **2007**, *7*, 5043–5059.
(8) Finlayson-Pitts, B. J.; Hemminger, J. C. *J. Phys. Chem. A* **2000**, *104*, 11463–11477.
(9) Finlayson-Pitts, B. J. *Chem. Rev.* **2003**, *103*, 4801–4822.
(10) Domine, F.; Shepson, P. B. *Science* **2002**, *297*, 1506–1510.
(11) Salvador, P.; Curtis, J. E.; Tobias, D. J.; Jungwirth, P. *Phys. Chem. Chem. Phys.* **2003**, *5*, 3752–3757.
(12) Minofar, B.; Vacha, R.; Wahab, A.; Mahiuddin, S.; Kunz, W.; Jungwirth, P. *J. Phys. Chem. B* **2006**, *2006*, 15939–15944.
(13) Liu, D.; Ma, G.; Levering, L. M.; Allen, H. C. *J. Phys. Chem. B* **2004**, *108*, 2252–2260.
(14) Kido Soule, M. C.; Blower, P. G.; Richmond, G. L. *J. Phys. Chem. A* **2007**, *111*, 3349–3357.
(15) Schnitzer, C. S.; Baldelli, S.; Shultz, M. J. *J. Phys. Chem. B* **2000**, *104*, 585–590.
(16) Xu, M.; Larentzos, J.; Roshdy, M.; Spinney, R.; Criscenti, L. J.; Allen, H. C. *Phys. Chem. Chem. Phys.* **2008**, *10*, 4793–4801.
(17) Marcus, Y.; Hefter, G. *Chem. Rev.* **2006**, *106*, 4585–4621.
(18) Lilley, T. H. Thermodynamic introduction to solute-solute and solute-solvent interactions in biological fluids. In *Handbook of Metal-Ligand Interactions in Biological Fluids. Bioinorganic Chemistry*; Berthon, G., Ed.; Marcel Dekker, Inc.: New York, 1995; Vol. 1.
(19) Hester, R. E.; Plane, R. A. *J. Chem. Phys.* **1966**, *45*, 4588–4593.
(20) Irish, D. E.; Walrafen, G. E. *J. Chem. Phys.* **1967**, *46*, 378–384.
(21) Wahab, A.; Mahiuddin, S.; Hefter, G.; Kunz, W.; Minofar, B.; Jungwirth, P. *J. Phys. Chem. B* **2005**, *109*, 24108–24120.
(22) Bertie, J. E.; Michaelian, K. H. *J. Chem. Phys.* **1998**, *109*, 6764–6771.
(23) Torii, H. *J. Phys. Chem. A* **2006**, *110*, 9469–9477.
(24) Vollmar, P. M. *J. Chem. Phys.* **1963**, *39*, 2236–2248.
(25) Li, X.-H.; Wang, F.; Lu, P.-D.; Dong, J.-L.; Wang, L.-Y.; Zhang, Y.-H. *J. Phys. Chem. B.* **2006**, *110*, 24993–24998.
(26) Jungwirth, P.; Tobias, D. J. *Chem. Rev.* **2006**, *106*, 1259–1281.
(27) Petersen, P. B.; Saykally, R. J. *Annu. Rev. Phys. Chem.* **2006**, *57*, 333–364.
(28) Chang, T. G.; Irish, D. E. *J. Phys. Chem.* **1973**, *77*, 52–57.

JP805376X